CONTRIBUTIONS to SCIENCE, **4** (2): 203-212 (2008)
Institut d'Estudis Catalans, Barcelona
DOI: 10.2436/20.7010.01.51 ISSN: 1575-6343
www.cat-science.com

Spin-orbit coupling and the electronic properties of quantum wires

Llorenç Serra
Departament de Física, Universitat de les Illes Balears
Institut de Física Interdisciplinària i de Sistemes Complexos IFISC (CSIC-UIB)

Resum

En aquest treball es revisen diversos resultats recents sobre la importància de la interacció espín-òrbita de Rashba per a l'estructura electrònica i la conductància de cables quàntics. Primerament es comenta com l'acoblament entre subbandes donat per la interacció de Rashba és crucial per a les energies de subbanda i les distribucions espacials d'espins, especialment en presència de camps magnètics. A continuació considerem el càlcul dels modes evanescents d'un cable quàntic, remarcant les peculiaritats degudes a la interacció d'espín-òrbita. Finalment, considerem el cas d'una interacció de Rashba localitzada, on fem la predicció de fortes ressonàncies de tipus Fano a la dependència de la conductància amb l'energia de l'electró incident. Aquestes ressonàncies s'observen més clarament a les transmissions de cada espín per separat. Trobem resultats numèrics exactes amb l'algorisme de frontera transmissora quàntica i resultats analítics amb un model simplificat de clara interpretació física.

Paraules clau: Interacció de Rashba, acoblament espín-òrbita, cables quàntics, teoria de massa efectiva, estats electrònics, conductància, espintrònica.

Abstract

We review recent work on the effects of the Rashba spin-orbit interaction on the electronic structure and the conductance of quantum wires. We first discuss the importance of the inter-subband coupling induced by the Rashba interaction for the wire subband-energies and spin distributions, especially in the presence of in-plane magnetic fields. We then consider the calculation of the evanescent modes, emphasizing the peculiarities of these states in the presence of spin-orbit coupling. Finally, we discuss the physical effects of a localized Rashba interaction in a quantum wire. We predict in this case the occurrence of Fano resonances in the dependence of the wire conductance with the incident electron energy. The Fano lineshapes manifest themselves more clearly in the spin-resolved transmissions. We obtain exact numerical results within the quantum-transmitting-boundary algorithm and also propose a simplified approach (the coupled-channel model) that captures the main ingredients of the effect and allows a more transparent physical interpretation.

Keywords: Rashba interaction, spin-orbit coupling, quantum wires, effective mass theory, electronic states, conductance, spintronics.

PACS numbers: 71.70.Ej, 72.25.Dc, 73.63.Nm

I. Introduction

When the two-dimensional (2D) electron gas lying at the interface of a semiconductor hetero-structure is further confined along one of the two directions, a quantum wire is formed. Today's nanolithographic techniques can manufacture quantum wires that have a high structural perfection and are largely free from impurities. These nanostructures are therefore close to ideal electron waveguides where propagation is allowed in one direction (along the wire) while, in the other directions, confinement induces the quantization of the energy states. The transverse quantization manifests itself in the formation of energy subbands occupied by electrons up to a maximum energy for a given wire density [1, 2].

Understanding the properties of electronic states in quantum wires is a central issue in nanoscience. In the ballistic regime, with low electronic densities, electron-electron interactions are not very important, and wire conductance is determined by the transmission of electrons as independent particles. This leads to the celebrated conductance quantization in multiples of the conductance quantum e^2/h, as predicted by Landauer [3] and measured in the narrow channels formed by quantum point contacts [4, 5]. Deviations from a perfect staircase quantization of the conductance can be due to various causes, such as impurities, localized states and spin-orbit interactions. The analysis of these deviations or 'anomalies' has been drawing much interest in nanoscience for many years [6–8].

This paper reviews several recent studies [9–12] carried out by our research group at the University of the Balearic Islands on the properties of semiconductor quantum wires. The main results and conclusions will be presented, but the reader is directed to the published references, and references therein, for additional details, discussions and bibliography. We shall focus on the role of the Rashba spin-orbit interaction [13] on the quantum wire properties. The Rashba interaction is a spin-orbit coupling originating in the inversion asymmetry of the quantum well in which the 2D electron gas in located. As a consequence of this asymmetry, there is a local electric field perpendicular to the quantum well plane that is responsible for the coupling between the 2D linear momentum and the spin of the electron. The effect is similar to the Pauli spin-orbit coupling in atomic physics but with the important difference that, while in an atom the electric field is that of the charged nucleus, here it is due to the quantum well's vertical asymmetry. Moreover, the intensity in the Rashba interaction is renormalized – and is relatively much more intense than in the atomic physics case– because effective values stemming from the host semiconductor energy bands are used [14].

Assuming a 2D electron gas lying in the xy plane, the Rashba interaction is described by the Hamiltonian,

$$\mathcal{H}_R = \frac{\alpha}{\hbar}\left(p_y\sigma_x - p_x\sigma_y\right) \ , \tag{1}$$

where $\vec{p} = (p_x, p_y)$ is the linear momentum and σ_x, σ_y are Pauli matrices. Interest in the Rashba spin-orbit interaction is mainly due to the fact that its intensity α can be tuned using external electrical gating. An α variability range of 5 to 10 meV nm has been demonstrated for InGaAs quantum wells in Ref. [15]. For GaAs, the coupling strength is, typically, an order of magnitude smaller because of the larger semiconductor band gap. The control of α constitutes the basis of many applications and devices in the emerging spintronics technology. Indeed, the Rashba interaction provides a mechanism for the controlled manipulation of the electron spin in semiconductor nanostructures. The spin transistor proposed by Datta and Das [16] is the most famous instance of a spintronics device based on the Rashba interaction. In this device, the electron transmission between ferromagnetic contacts is manipulated by means of the spin rotation induced by the Rashba interaction as the electrons propagate in the channel connecting the two ferromagnets. In addition to spin transistors, spin filters based on the Rashba interaction as well as detectors of entangled electron pairs and of hyperfine nuclear dynamics have also been proposed [17–19].

The electronic states in a wire are usually classified as propagating or evanescent. While the former are physically realizable throughout wire, the latter can only be found in restricted domains, close to possible interfaces and inhomogeneities in the system. Although the evanescent states cannot be seen in a perfectly clean wire, finding their wavenumbers and their energy subbands is very important because these aspects determine the physics when any impurity or inhomogeneity is added to the wire [20]. As we shall discuss, the presence of the spin-orbit coupling makes the determination of evanescent states highly non-trivial. An algorithm recently proposed in our group and a specific application (a potential step in the wire) are discussed below [12].

Since the Rashba intensity can be varied using external electric fields induced by miniaturized electrodes, it is natural to consider the possibility of non-homogeneous Rashba intensity, when α becomes position-dependent. This situation has been investigated in various geometries, such as a constant Rashba strength in a semiplane, a stripe and a dot [21–24]. Here we shall discuss the case of a Rashba dot that is traversed by a quantum wire [10, 11]. Remarkably, the Rashba dot sustains localized states that couple with the wire propagating states, modifying the wire-conductance quantization with conspicuous Fano resonances at specific energies. The two terms in Eq. (1) are responsible for the formation of quasibound states in the Rashba dot region and their coupling with the wire propagating states. As we shall discuss below, the underlying physics is nicely accounted for by the coupled-channel model (CCM).

The paper is organized as follows. Section II is devoted to the case of a wire with extended spin-orbit coupling that is uniform throughout the system. We first analyze the modification of the propagating subbands and the associated spatial spin textures in the presence of in-plane magnetic fields. Then, we analyze the evanescent modes and a specific example of application (namely, the potential step). Section III deals with the localized spin-orbit coupling. Finally, Section IV presents our conclusions.

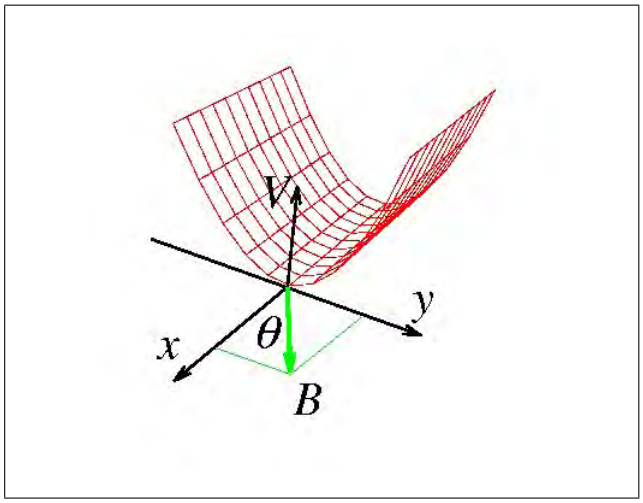

Figure 1. Schematic representation of the wire potential $V(y) = m\omega_0^2 y^2/2$ and magnetic field orientation considered in this work. From Ref. 9, "Copyright (2005) by the American Physical Society".

II. Extended Rashba coupling

Let us assume that α takes a constant value for all points of the xy plane and that the confinement is parabolic in the y direction,

$$V(y) = \frac{1}{2}m\omega_0^2 y^2 \ . \tag{2}$$

The wire orientation, then, is along x. In addition, an in-plane magnetic field $\vec{B} = (B\cos\theta, B\sin\theta)$ acts through the Zeeman Hamiltonian (see Fig. 1)

$$\mathcal{H}_Z = g\mu_B B(\cos\theta\sigma_x + \sin\theta\sigma_y)/2 \ . \tag{3}$$

Orbital magnetic effects are absent in this geometry since they arise only from perpendicular fields. Adding all contributions, the resulting Hamiltonian reads

$$\mathcal{H} = (p_x^2 + p_y^2)/2m + V(y) + \mathcal{H}_Z + \mathcal{H}_R \; . \qquad (4)$$

In Eqs. (2,3,4), m and g represent, respectively, the effective values for the mass and gyromagnetic ratio of the conduction-band electrons in the host semiconductor. We shall take the GaAs values $g = -0.44$ and $m = 0.067m_e$, with m_e the bare-electron mass, for these parameters. We also stress that a natural units system for parabolic wires is set by the transverse oscillator. This amounts to measuring energies in units of $\hbar\omega_0$ and lengths in units of the oscillator length $\ell_0 = \sqrt{\hbar/m\omega_0}$.

In the absence of $\mathcal{H}_R$, the transverse modes are pure oscillator functions and the energy subbands are quadratic in the wave-number k associated with p_x, the linear momentum along the wire. The two terms in $\mathcal{H}_R$, Eq. (1) are usually named according to the modifications made to this simplified scenario. The term $\mathcal{H}_R^{(1)} \equiv -\alpha p_x \sigma_y/\hbar$ is called the Rashba precession (RP) term because it is diagonal in k and acts similarly to a k-dependent magnetic field along y, forcing spin precession for spins in arbitrary orientations. The second spin-orbit term $\mathcal{H}_R^{(2)} \equiv \alpha p_y \sigma_x/\hbar$ is the Rashba intersubband coupling (RIC), with p_y connecting adjacent oscillator transverse modes and σ_x inducing spin flip for spins along y, the RP term spin axis.

A. Relevance of RIC

For large wavenumber values the RP term obviously dominates over RIC since it grows with k while the latter does not depend explicitly on k. Importantly, when RIC is neglected, the Schrödinger equation can be analytically solved. This analytical solution has motivated many studies in the literature. In Ref. 9, our group proved that neglecting RIC is a delicate approach, which is not generally justified for low and intermediate wavenumber values. This subsection reviews this result.

In the absence of RIC, the Schrödinger equation $\mathcal{H}\Psi(x,y,\eta) = E\Psi(x,y,\eta)$, where $\eta = \uparrow, \downarrow$ is the spin double-valued variable, is analytically solved by the spinorial wavefunctions

$$\Psi \equiv \Psi_{nks} = \phi_n(y)\frac{e^{ikx}}{\sqrt{2}}\begin{pmatrix} e^{i\Omega_k/2} \\ s\, e^{-i\Omega_k/2} \end{pmatrix} \; . \qquad (5)$$

In Eq. (5), $\phi_n(y)$ is the 1D oscillator wave function, solution of the equation $[p_x^2/2m + V(y)]\phi_n = \varepsilon_n\phi_n$, with $\varepsilon_n = (n-1/2)\hbar\omega_0$, $n = 1, 2, \ldots$. As mentioned above k is the x wave number and $s = \pm 1$ gives a spin branching number. The three quantum numbers are therefore (nks). The angle Ω_k, determining the orientation of the spin in the xy plane, is the argument of the complex number $z_k \equiv g\mu_B B e^{i\theta}/2 + i\alpha k$. The two contributions in z_k stem from the Zeeman term and the spin-orbit coupling, respectively. Notice that the Zeeman term tends to align the spinor in the direction of the field, given by the angle θ, while the Rashba coupling favors alignment along y. The analytical eigenenergies are

$$E \equiv E_{nks} = \varepsilon_n + \frac{\hbar^2 k^2}{2m} + s|z_k| \; . \qquad (6)$$

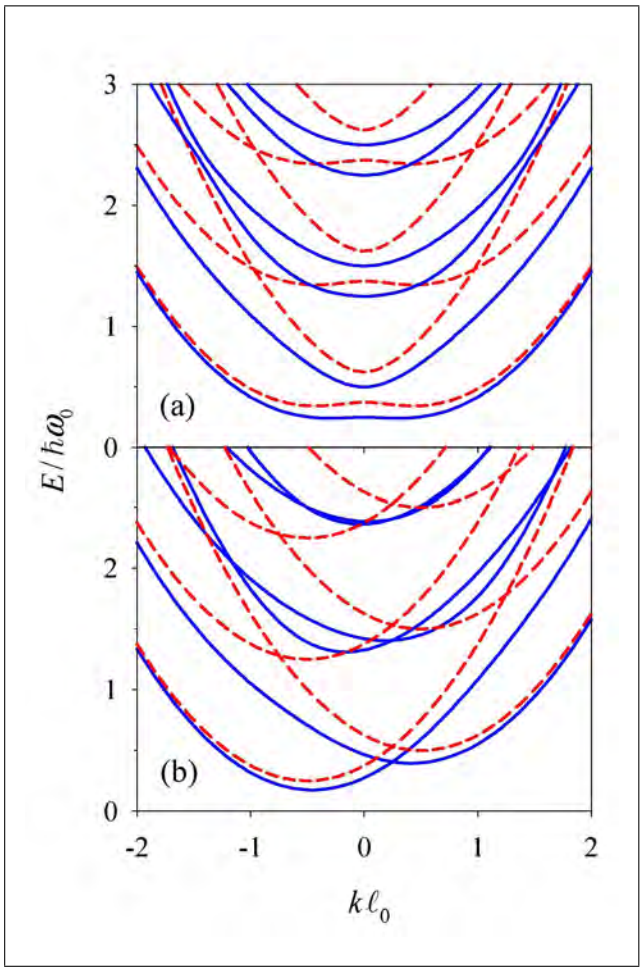

Figure 2. (a) Dispersion relation for $\theta = 0$, $g\mu_B B = 0.25\hbar\omega_0$ and $\alpha = 0.5\hbar\omega_0\ell_0$. The solid line corresponds to the case where the RIC is included, while the dashed line shows the case without it. (b) Same as (a) for $\theta = \pi/2$. From Ref. 9, "Copyright (2005) by the American Physical Society."

When RIC is added to the above picture, the solution is, in general, no longer analytical. It can be obtained numerically. Figure 2 compares the energy subbands of the full Hamiltonian (solid) with those in the absence of RIC (dashed) for a chosen magnetic field oriented along $\theta = 0$ (upper panel) and $\theta = \pi/2$ (lower). Important modifications due to RIC are the transformation of the crossings around $k\ell_0 = 1$ in anticrossings and the reduction, or even disappearance in upper subbands, of the local maxima at $k = 0$ (upper panel). Notice also that around $k = 0$ there is a downwards shift due to repulsion with upper subbands.

The modification of the energy subbands has important consequences for the wire properties. RIC also causes modifications on the spin spatial distributions. While Eq. (5) had good spin states, with spin oriented at an angle Ω_k in the xy plane, inclusion of RIC causes a spin texture, with a y-dependent distribution of non-parallel spins. Indeed, the existence of clear spin textures is a signature of the RIC term. The local spin components for the lowest subband at three different propagation momenta are shown in the upper plots of Figure 3. While all in-plane spins are essentially collinear, a sizeable z-component,

similar in magnitude to the in-plane one, precludes the definition of a common spin axis when $k\ell_0 \neq 0$ and thus shows the importance of RIC. The local z-magnetization in real space $\langle\sigma_z(y)\rangle$ is antisymmetric in y, which leads to a vanishing integrated $\langle\sigma_z\rangle$ [25] and gives rise to spin accumulations at the wire edges, which are reminiscent of the intrinsic spin Hall effect [26]. Here, however, the effect arises in a confined system [27].

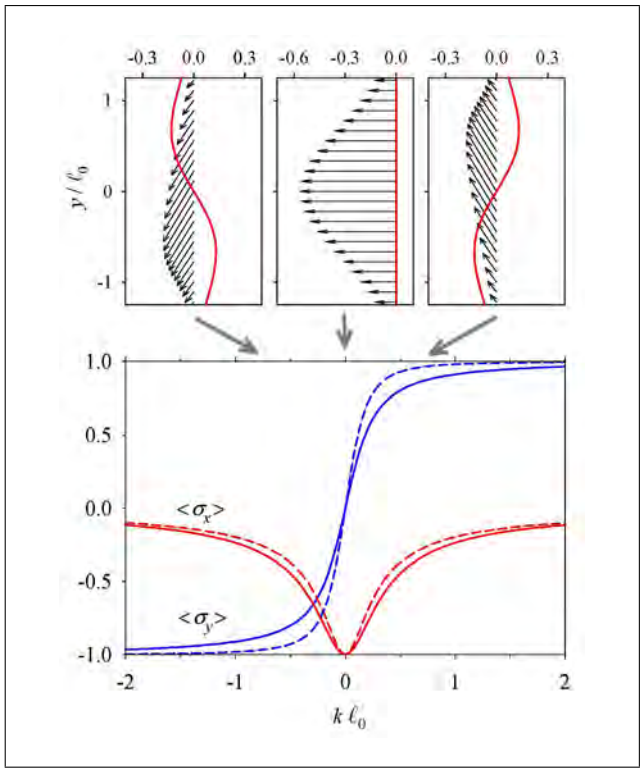

Figure 3. Lower plot: Dependence on k of the spin expectation values in the lowest subband. The solid lines are obtained when both Rashba terms are included, while the dashed lines are the results when RIC is neglected. We set $g\mu_B B = 0.2\hbar\omega_0$, $\alpha = 0.5\hbar\omega_0\ell_0$ and $\theta = 0$. The upper panels display the spin texture for three selected propagation momenta, taking into account both Rashba terms. The $k\ell_0$ values (indicated by the thick arrows pointing to the k-axis) are -0.75, 0 and 0.75 for the left, center and right upper plots, respectively. The vector plot shows the in-plane spin and the continuous line corresponds to the z-component. From Ref. 9, "Copyright (2005) by the American Physical Society".

In Ref. 9, the linear conductance $\mathcal{G}$ as a function of energy and Rashba intensity was analyzed. Figure 4 shows this result for an orientation of the magnetic field of $\theta = 0$. When RIC is not included, $\mathcal{G}$ alternates, with increasing energy, steps of $+2e^2/h$ with downward jumps of $-e^2/h$ due to the presence of maxima in the lower subbands. When RIC is included, two major modifications are apparent: a) stronger Rashba couplings are needed to observe the alternate steps of $+2e^2/h$ and $-e^2/h$, and b) in any case, this anomalous pattern of steps vanishes when the Fermi energy increases. In particular, as shown by the insets, when $\alpha = \hbar\omega_0\ell_0$, the sequence of conductance steps in units of $\mathcal{G}_0$ is $+2, -1, +1, +2, -1, +1, \ldots$ when RIC is neglected and $+2, -1, +1, +1, +1, \ldots$ when it is included. Therefore, Figure 4 proves that, in order to observe the modifications of the linear conductance steps due to the Rashba interaction, it is essential to have a relatively low Fermi energy or, equivalently, a rather small number of propagating modes. Nevertheless, the stronger the value of α, the higher the plateau containing anomalous conductance variations.

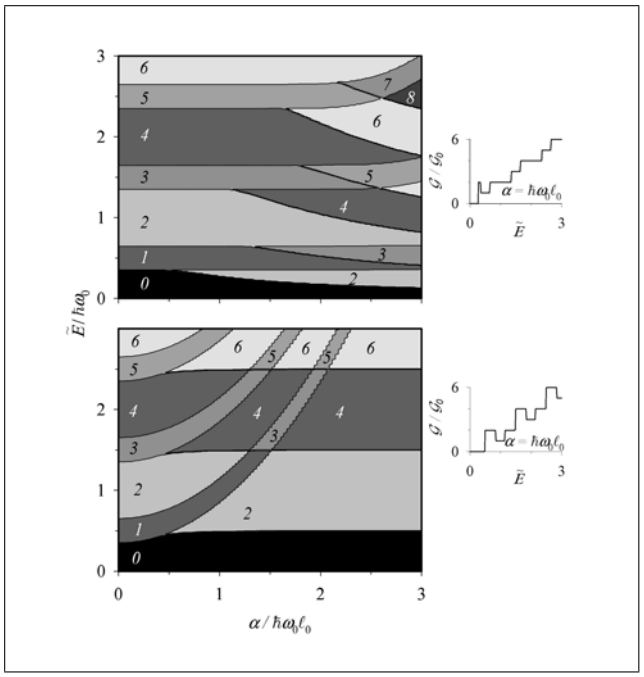

Figure 4. Variation of the conductance with Rashba intensity and the Fermi energy E in the full Rashba model (upper panel) and neglecting RIC (lower panel). We set $g\mu_B B = 0.3\hbar\omega_0$ and parallel magnetic field $\theta = 0$. A rigid shift with Rashba intensity has been taken into account to define $\tilde{E}/\hbar\omega_0 = E/\hbar\omega_0 + \frac{1}{2}(\alpha/\hbar\omega_0\ell_0)^2$. The numbers in the plateaus give the conductance in units of the conductance quantum. On the right, small plots show vertical cuts of the corresponding figures on the left for the given values of α. $\mathcal{G}_0 \equiv e^2/h$ is the conductance quantum. From Ref. 9, "Copyright (2005) by the American Physical Society".

B. Evanescent modes

The preceding subsection discussed the wire subbands associated with the propagating modes, with real wave numbers k in Eq. (5). When k is complex, the corresponding modes are called evanescent because the imaginary part $\mathrm{Im}(k)$ gives an exponential factor causing decay along the wire. Obviously, the decay can be seen as a divergence for the reversed direction. These modes are therefore not physically realizable in the entire channel for x spanning the interval $(-\infty, +\infty)$. Nevertheless, they are extremely important because many physical states do behave as evanescent in restricted domains.

In this subsection, we shall focus, for simplicity, on the $B = 0$ case. As in Eq. (5), the spinorial wavefunction is assumed to be separable in the following form:

$$\Psi(x, y, \eta) \equiv \phi(y, \eta)e^{ikx} \ . \tag{7}$$

Let us now express the spin- and y-dependent part in terms of the eigenspinors of σ_x, $\chi_{x\pm}(\eta)$, as

$$\phi(y, \eta) \equiv \phi_1(y)\chi_{x+}(\eta) + \phi_2(y)\chi_{x-}(\eta) \ . \tag{8}$$

The Schrödinger equation $(\mathcal{H}-E)\Psi(x,y,\eta)=0$ can be recast as a matrix equation for the amplitudes $\phi_{1,2}(y)$,

$$\begin{pmatrix} h_0 - i\alpha\frac{d}{dy} + \frac{\hbar^2k^2}{2m} - E & -i\alpha k \\ i\alpha k & h_0 + i\alpha\frac{d}{dy} + \frac{\hbar^2k^2}{2m} - E \end{pmatrix} \times \times \begin{pmatrix} \phi_1(y) \\ \phi_2(y) \end{pmatrix} = 0 \,, \tag{9}$$

where we have defined the transverse oscillator operator

$$h_0 \equiv -\frac{\hbar^2}{2m}\frac{d^2}{dy^2} + \frac{1}{2}m\omega_0^2 y^2 \,. \tag{10}$$

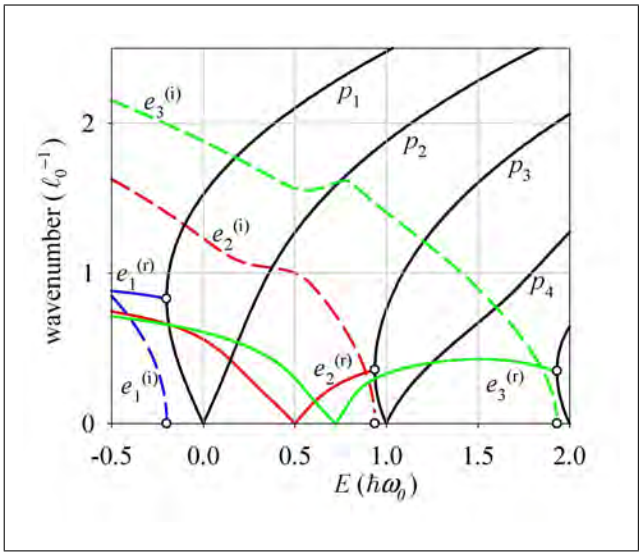

Figure 5. Mode dispersion for $\alpha = \hbar\omega_0\ell_0$. The branch labels indicate mode number n as well as evanescent or propagating character as e_n and p_n, respectively. In the case of evanescent modes, superindexes (r) and (i) indicate whether the branch gives the real or imaginary part of the wavenumber. Open circles indicate the position of the threshold energies $E_n^{(th)}$ where the $e_n^{(i)}$ branches disappear while the $e_n^{(r)}$ branches join with a propagating mode $p_{n'}$. From Ref. 12, "Copyright (2007) by the American Physical Society".

Equation (9) determines the evanescent mode wavefunctions and wave-numbers. Although it has the formal appearance of a linear eigenvalue equation with eigenvalue E, in our case the energy is given and the wavenumber k is unknown. Notice also that, for complex k's, the matrix in Eq. (9) in non-Hermitian, which prevents the use of standard matrix diagonalization routines. This invalidates the computational strategy normally used for propagating modes, which consists in: a) preassign a value to k; b) diagonalize (9); c) find *a posteriori* what k's give as eigenvalues the energy of interest E.

In Ref. 12 our group proposed an algorithm to solve Eq. (9) and therefore determine the wire evanescent modes. The reader is referred to that reference for the details of the method. Here, we shall only briefly discuss some general properties of the evanescent subbands. Figure 5 shows the mode dispersion for a selected wire with strong Rashba coupling. We only plot positive wavenumbers, noting that, due to symmetry, signs of either $\mathrm{Re}(k)$ or $\mathrm{Im}(k)$ can be inverted, giving a four-fold degeneracy of each evanescent mode and a two-fold degeneracy of the propagating ones.

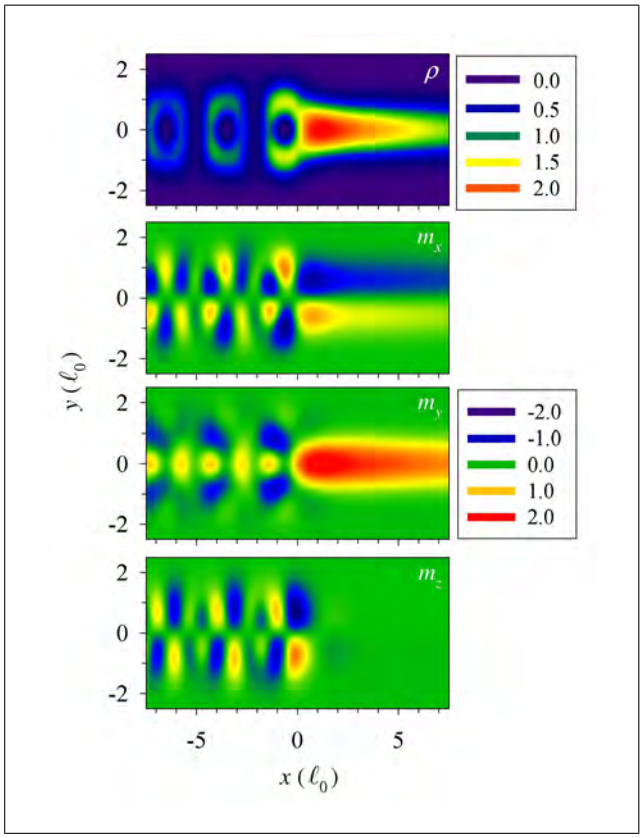

Figure 6. Density ρ and spin magnetization (m_x, m_y, m_z) distributions in a wire with a potential step at $x=0$ of $V_0 = 1.13\hbar\omega_0$ and having $\alpha = \hbar\omega_0\ell_0$. The density contour numerical values are given in units of ℓ_0^{-2} while those of magnetization density are given in units of $\hbar/(2\ell_0^2)$. Incidence is from the left in mode p_1 shown in Figure 5, for an energy $E = 0.93\hbar\omega_0$ slightly below the threshold for propagating modes p_3 and p_4. From Ref. 12, "Copyright (2007) by the American Physical Society".

Mode degeneracies can be explained by taking into account that if a solution to Eq. (9) is characterized by a given wavenumber and amplitudes $\{k, \phi_1, \phi_2\}$ then, by simply taking the complex conjugate of Eq. (9), we find a solution having $\{k^*, \phi_2^*, \phi_1^*\}$. Moreover, our starting Hamiltonian $\mathcal{H}$ is time reversal invariant, which, for a spin 1/2 system, implies that the solutions must appear in degenerate pairs of time-reversed states known as Kramers doublets. Using the time-reversal operator for a spin 1/2 system, $\Theta = -i\sigma_y\mathcal{K}$, where $\mathcal{K}$ represents complex conjugation, we find the Kramers partner of $\{k, \phi_1, \phi_2\}$ as $\{-k^*, \phi_2^*, -\phi_1^*\}$. In summary, with both complex conjugation (cc) and time-reversal symmetry, we obtain the four-fold degeneracy

$$\begin{array}{ccc} \{k, \phi_1, \phi_2\} & \overset{cc}{\longleftrightarrow} & \{k^*, \phi_2^*, \phi_1^*\} \\ \Theta\updownarrow & & -\Theta\updownarrow \\ \{-k^*, \phi_2^*, -\phi_1^*\} & \overset{cc}{\longleftrightarrow} & \{-k, -\phi_1, \phi_2\} \,. \end{array} \tag{11}$$

In Figure 5, the dispersion of the propagating modes p_n shows a familiar picture (discussed in the preceding subsection). There is a threshold energy $E_n^{(th)}$ for the activation of

the n-th propagating mode. Due to the spin-orbit coupling, when E slightly exceeds $E_n^{(th)}$, propagating states with nonzero wavenumber $k_n^{(th)}$, belonging to the n-th mode, are allowed. For E slightly below $E_n^{(th)}$, there is an evanescent mode whose $\mathrm{Im}(k)$ approaches zero as E approaches $E_n^{(th)}$, as shown by the $e_n^{(i)}$ branches of Figure 5. The real parts $\mathrm{Re}(k)$ of the evanescent wavenumbers, $e_n^{(r)}$ branches, display some oscillations and evolve from evanescent to propagating modes as E crosses the threshold value $E_n^{(th)}$.

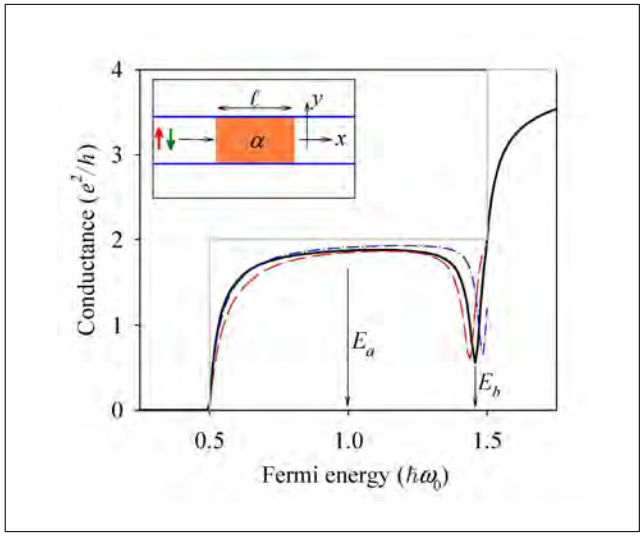

Figure 7. Conductance for a Rashba dot of $\ell = \ell_0$ and $\alpha_0 = 0.75\hbar\omega_0\ell_0$ in the exact (solid), numerical CCM (dashed) and analytical CCM (dash-dotted) calculations. The solid gray line shows the case without the Rashba dot and the inset shows the physical system. From Ref. 11, "Copyright (2007) by the Institute of Physics".

The interest in the evanescent modes lies in the fact that knowledge of them allows the analysis of many different inhomogeneities. In Ref. 12, the case of a potential step $V_0\Theta(x)$ was presented as an illustrative example. Electrons incident from the left ($x < 0$) impinge on the step border and, assuming their energy is not enough to allow for propagation in the right region ($x > 0$), only pure evanescent modes will be seen for $x > 0$. At the step edge, the wave functions must match adequately, as this condition determines the amplitudes of the reflected propagating modes for $x < 0$ and of the evanescent waves for all x. Figure 6 shows the density and spin magnetizations obtained after solving the linear system of equations corresponding to the matching conditions. The spatial distribution of density and magnetization due to evanescent modes are clearly seen for $x > 0$, while on the left side there are marked interference effects between the coexisting modes. Focusing on the evanescent mode side, there is a strong injection of spin y magnetization m_y, clearly due to the fact that the incident mode p_1 is mostly polarized along $+y$ (it is not completely polarized due to the admixture induced by the RIC term). There is also a significant accumulation of evanescent m_x magnetization, of different signs on either side of the wire. Had we considered incidence from mode p_2 at the same energy, the spin magnetizations would have been reverted with respect to those shown in Figure 6, indicating that the average incidence from the two modes p_1 and p_2 does not produce any net magnetization, not even locally. On the contrary, the density shown in the upper panel of Figure 6 is the same for incidence from either mode.

III. Localized Rashba coupling

In this section we analyze the case of a Rashba spin-orbit coupling whose intensity is position-dependent $\alpha(\mathbf{r})$. For simplicity, we shall consider the case of $\alpha(x) = \alpha_0$ (constant) for $0 < x < \ell$ and zero elsewhere. In this section, we also assume that no magnetic field is present. The physical system is, then, a parabolic quantum wire traversing a region of length ℓ with spin-orbit coupling, which we call the Rashba dot (see inset in Figure 7). In order to retain good mathematical properties, the Hamiltonian is presently symmetrized with its Hermitian conjugate (H.c.)

$$\mathcal{H}_R = \frac{\alpha(x)}{2\hbar}\left(p_y\sigma_x - p_x\sigma_y\right) + \mathrm{H.c.}\,. \qquad (12)$$

We review the results of Refs. 10, 11, which showed, with numerical and analytical calculations, that the present geometry leads naturally to the appearance of Fano resonance profiles in the energy dependence of the conductance. The resonances depend quite sensitively on the the Rashba dot's properties, such as its dimensions and SO intensity. We named this influence of the Rashba SO coupling on the wire conductance the Fano-Rashba effect.

A. The Fano-Rashba effect

Fano resonances [28] are a general phenomenon that has been observed in different fields, such as atomic physics [29], Raman scattering [30] and mesoscopic electron transport [31]. Fano-resonance physics appears wherever there is interference between two paths, one corresponding to direct transmission and the other to the passage through a quasi-bound state lying nearby in energy. As a consequence, characteristic asymmetric lineshapes appear in the most general case, with conductance dips in which transmission is greatly quenched. Indeed, for the case of scattering centers that may be modeled as attractive potentials it was shown that an exact transmission zero should always be present [6, 7]. In our case of a Rashba dot, the existence of transmission zeros is not always guaranteed. Only for some specific dimensions and intensities of SO coupling does the wire conductance vanish at the dip position.

Figure 7 shows a typical conductance curve for specific values of α and ℓ numerically obtained using finite differences in the quantum-transmitting-boundary algorithm [10, 32]. The usual staircase conductance is modified because of the Rashba dot in two main aspects. First, the initial part of the step is smoothed (a usual quantum behavior of scattering through potential wells). Second, a pronounced conductance dip appears near the end of the conductance plateau.

As mentioned above, the existence of conductance dips is normally due to quasibound states. To prove it in the present context, we show in Figure 8 the wave-function for two different energies, E_a and E_b, where E_a is chosen to lie in the smooth

conductance region while E_b corresponds precisely to the dip position. Indeed, at energy E_b, the wave function strongly resonates within the Rashba dot and is so amplified that it greatly exceeds the values in the leads. This explicitly shows the dramatic influence of the quasibound state. A systematic analysis of the dip positions for varying α's and ℓ's was performed in Ref. 10. Figure 9 displays the variation of the linear conductance when the Rashba intensity α and the length of the Rashba dot ℓ vary. Importantly, we observe dips going all the way down to zero within numerical precision for specific values of these parameters. In Figure 9(a), we show how, for a fixed value of E, the resonances can be tuned by varying α, which may be regarded as a gate voltage. This is a central prediction of Ref. 10 that can be tested experimentally.

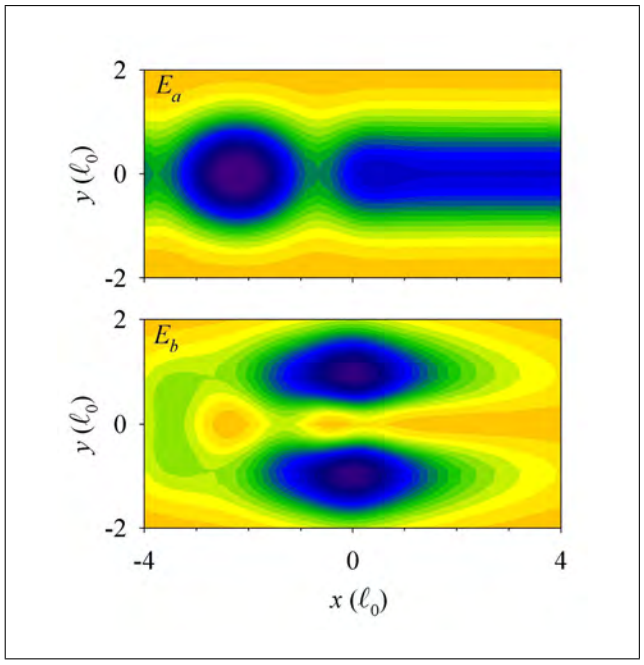

Figure 8. Probability densities for the energies E_a (upper) and E_b (lower) shown in Figure 7. Darker means higher probability. From Ref. 11, "Copyright (2007) by the Institute of Physics".

B. The coupled-channel model (CCM)

The physics behind the results shown in the preceding subsection is more easily analyzed within the CCM. Assume the following expansion of the electron wave-function $\Psi(x,y,\eta)$, in the transverse oscillator modes $\phi_n(y)$ and spin eigenstates $\chi_\pm(\eta)$ of σ_y,

$$\Psi(x,y,\eta) = \sum_{n,s=\pm} \psi_{ns}(x)\phi_n(y)\chi_s(\eta)\ . \qquad (13)$$

Substituting Eq. (13) into the Schrödinger equation $H\Psi = E\Psi$ and projecting onto the functions $\phi_n\chi_s$, we obtain the CCM equations for the various channel amplitudes $\psi_{ns}(x)$. We shall restrict to the first conductance plateau, i.e., to electron energies fulfilling $\varepsilon_1 < E < \varepsilon_2$, and also truncate the expansion in Eq. (13) to the first two transverse modes $n = 1, 2$. The selection rules stemming from the Rashba interaction require spin flip and also $\Delta n = \pm 1$. Therefore, we obtain two independent two-band models, with ψ_{1+} coupled to ψ_{2-} and ψ_{1-} to ψ_{2+}. Actually, the two models are equivalent and we shall focus for simplicity on the ψ_{1+}–ψ_{2-} system.

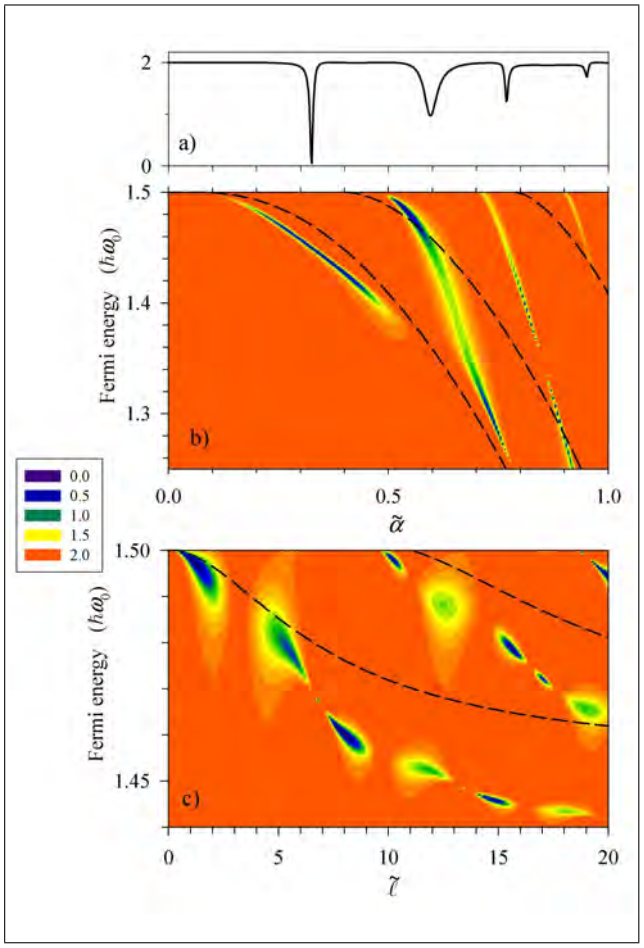

Figure 9. Linear conductance for energies close to the onset of the second plateau $\varepsilon_2 = 1.5\hbar\omega_0$. (a) Conductance as a function of the Rashba strength $\tilde{\alpha} \equiv \alpha/\hbar\omega_0\ell_0$ for a fixed Fermi energy $E = 1.45\hbar\omega_0$ and a fixed dot size $\tilde{\ell} \equiv \ell/\ell_0 = 8$. (b) Dependence of the conductance with $\tilde{\alpha}$ for a fixed dot size $\tilde{\ell} = 8$. (c) Conductance as a function of the dot size for $\tilde{\alpha} = 0.3$. Dashed lines show the 1D bound state energies relative to ε_2. From Ref. 10, "Copyright (2006) by the American Physical Society".

The CCM equations for the ψ_{1+}, ψ_{2-} amplitudes are greatly simplified by means of the gauge transformation $\psi_{1+,2-} \to \psi_{1+,2-}\exp(\pm i\int^x k_R(x')dx')$, where we have defined $k_R(x) = m\alpha(x)/\hbar^2$. The resulting CCM system then reads

$$\left[\frac{p_x^2}{2m} - \frac{\hbar^2 k_R^2}{2m} - E + \varepsilon_1\right]\psi_{1+} = V_{12}\psi_{2-}\ , \qquad (14)$$

$$\left[\frac{p_x^2}{2m} - \frac{\hbar^2 k_R^2}{2m} - E + \varepsilon_2\right]\psi_{2-} = V_{21}\psi_{1+}\ . \qquad (15)$$

The left-hand sides of Eqs. (14) and (15) constitute the channel background problems. They are 1D Schrödinger equations for a potential well $-\hbar^2 k_R(x)^2/2m$, the only difference being that the energy is positive (negative) for ψ_{1+} (ψ_{2-}). This clearly shows the propagating and evanescent character of the two channels,

respectively. The right-hand sides contain the channel couplings, with the mixing potentials

$$V_{12}(x) = V_{21}^*(x) = \frac{i}{\hbar}\langle\phi_1|p_y|\phi_2\rangle\alpha(x)e^{2i\int^x k_R(x')dx'} \ . \quad (16)$$

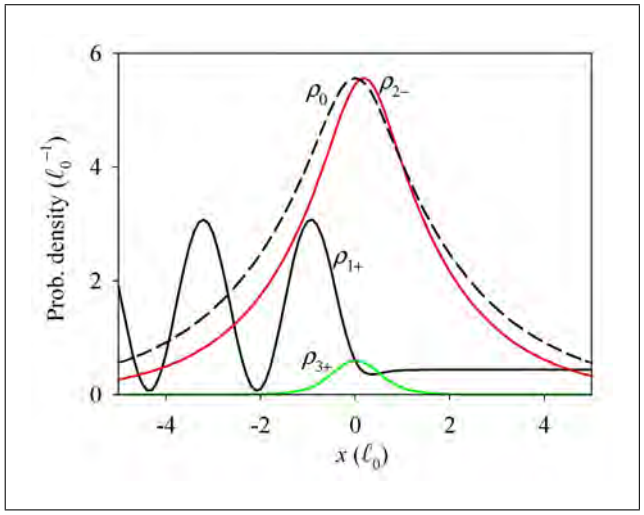

Figure 10. Channel probability densities within CCM, defined as $\rho_{ns}(x) = |\psi_{ns}(x)|^2$, for the energy E_b of Figure 7. The probability density corresponding to the background bound state $\rho_0(x) = |\phi_0(x)|^2$ is also shown. $\rho_0(x)$ has been arbitrarily rescaled in order to reproduce the peak height of $\rho_{2-}(x)$ for better comparison. From Ref. 11, "Copyright (2007) by the Institute of Physics".

The dashed line in Figure 7 shows the conductance from the full solution of Eqs. (14) and (15), obtained numerically. Clearly, the existence of the conductance dip is well reproduced by the CCM. However, a more transparent physical interpretation is obtained with an *ansatz* solution. Indeed, the evanescent character of ψ_{2-} in Eq. (15) motivates the ansatz $\psi_{2-}(x) \propto \phi_0(x)$, where ϕ_0 is the background bound state fulfilling $\left(p_x^2/2m - \hbar^2k_R^2/2m - \varepsilon_0\right)\phi_0 = 0$, with $\varepsilon_0 < 0$. Since $E > \varepsilon_1$, Eq. (14) describes a 1D scattering process with a source term given by $V_{12}\psi_{2-}$ and asymptotic wave vector $k = \sqrt{2m(E-\varepsilon_1)/\hbar^2}$. Using Green's function G, given in terms of the background asymptotic states φ_r and φ_l behaving as $te^{\pm ikx}$ for $x \to \pm\infty$, respectively, we find the total transmission

$$\begin{aligned} T_+(E) &= |t|^2 \frac{(E-\varepsilon_2-\varepsilon_0-\Delta+\delta)^2+(\gamma-\Gamma)^2}{(E-\varepsilon_2-\varepsilon_0-\Delta)^2+\Gamma^2} \\ &\equiv |t|^2 \frac{|\epsilon+q|^2}{\epsilon^2+1} \ , \end{aligned} \quad (17)$$

where we have defined

$$\Delta + i\Gamma \equiv \langle\phi_0|V_{21}GV_{12}|\phi_0\rangle \ , \quad (18)$$

$$\delta + i\gamma \equiv \frac{m}{i\hbar^2kt}\langle\varphi_l^*|V_{12}|\phi_0\rangle\langle\phi_0|V_{21}|\varphi_r\rangle \ . \quad (19)$$

The last expression in Eq. (17) emphasizes the generalized Fano lineshape, with $\epsilon = (E-\varepsilon_2-\varepsilon_0-\Delta)/\Gamma$ and $q = \delta/\Gamma + i(\gamma/\Gamma - 1)$. In general, the Rashba dot yields complex q's. Therefore, the factor $|\epsilon + q|$ in Eq. (17) cannot vanish at any ϵ, or equivalently any E, thus hindering the formation of zero-transmission dips. For some particular values of α and ℓ, however, we have shown above that there are *accidental* cases where the conductance dip is compatible with a zero value within numerical precision [10]. As shown by the dash-dotted line of Figure 7, the ansatz solution satisfactorily reproduces the conductance dip although, of course, there are some minor discrepancies with the exact solution (solid line).

As mentioned above, the exact solution of the CCM equations can be obtained numerically, using a 1D formulation of the quantum-transmitting-boundary algorithm. This allows a check on the validity of the ansatz $\psi_{2-}(x) \propto \phi_0(x)$. Figure 10 shows the different channel amplitudes (including the ψ_{3+} channel), as well as the bound state ϕ_0, for the dip energy E_b of Figure 7. The probability density for channel ψ_{1+} does not vanish for $x \to \infty$, thus proving the propagating nature of this channel, although transmission is rather low at this energy. There is good qualitative agreement of the probability densities ρ_{2-} and ρ_0, which explicitly proves that the ansatz is indeed a reasonable assumption for the evanescent channels. The numerical solution was obtained by also including channel ψ_{3+}. However, the smallness of ρ_{3+} with respect to the other channel densities supports the truncation to the lowest two modes.

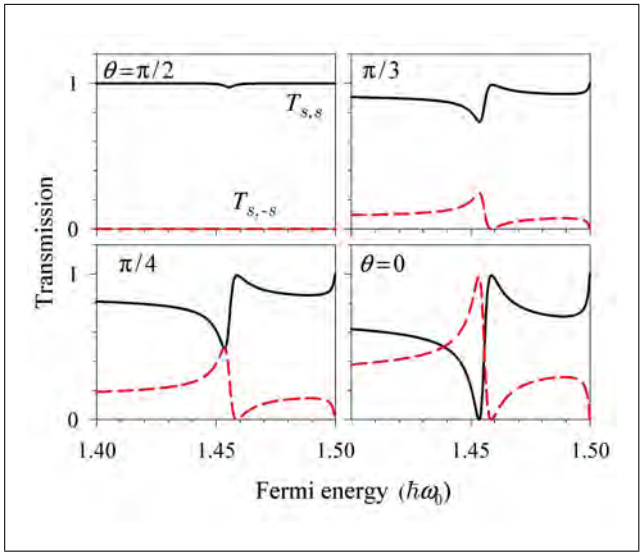

Figure 11. Spin dependent transmissions for $\alpha = 0.3\hbar\omega_0\ell_0$ and $\ell = 9.5\ell_0$ when the spin quantization rotates from y ($\theta = \pi/2$) to x ($\theta = 0$). The total transmission $T = \sum_{s,s'} T_{s,s'}$ is the same in all cases. From Ref. 10, "Copyright (2006) by the American Physical Society".

Thus far, we have taken the spin quantization axis along y, for which both spin channels are equivalent and uncoupled, i.e., $T_+ = T_-$, and there is no spin flip. This is not true along other orientations and, generally, one must consider the four contributions to the total transmission $T = \sum_{s,s'} T_{s,s'}$, where s denotes the spin state in the left lead (incident) and s' that of the right lead (transmitted). Obviously, for the present case, where the absence of magnetic fields preserves spin rotational invariance, T does not depend on the chosen quantization axis. Furthermore, due to time reversal symmetry, we always have $T_{++} = T_{--}$ and $T_{+-} = T_{-+}$ [33]. In Figure 11, we show the spin-resolved transmissions when the spin axis is rotated on

the plane from $\theta = \pi/2$ (y-axis) down to 0 (x-axis). Quite remarkably, $T_{s,s}$ and $T_{s,-s}$ develop conspicuous Fano lineshapes with exact transmission zeros for $T_{s,-s}$ as θ decreases, even for cases in which the total transmission has a vanishingly small dip. Therefore, experiments using ferromagnetic leads with tilted spin orientation would greatly enhance the Fano lineshapes.

We end this section by mentioning two lines in which our group is currently extending the research on local Rashba couplings. One considers magnetic fields and how they influence the Fano-Rashba effect mentioned above. In particular, we are analyzing the interplay of the Zeeman gap with the local Rashba coupling due to an in-plane magnetic field [34]. Another line of research deals with the effects due to electron-electron interaction. In this respect, we have already proved that a local Rashba dot can, in the appropriate range of parameters, display pure interaction effects such as Coulomb blockade and Kondo correlations, manifested as current oscillations [35].

IV. Conclusions

We reviewed several recent studies carried out at the University of the Balearic Islands to analyze the spectrum, magnetization distributions and linear transport of ballistic quantum wires in the presence of extended Rashba interaction and in-plane magnetic fields. The crucial importance of RIC for these properties was stressed. At strong spin-orbit coupling, the modifications in the energy subbands include the appearance of sizeable shifts, anticrossings and large reductions on the subband maxima. The changes in subband structure lead to precise predictions for measurements of the linear transport properties, such as a severe reduction on the anomalous conductance steps when $\theta = 0$ and a nontrivial dependence of the steps on the Rashba intensity.

Besides the abovementioned propagating states, we also considered the wire's evanescent modes, characterized by complex wavenumbers with both real and imaginary parts. Due to symmetry, one can invert the signs of either $\mathrm{Re}(k)$ or $\mathrm{Im}(k)$, or both, and still obtain physically valid wavenumbers. Typically, when energy is decreased the wire modes evolve from propagating to evanescent as the energy crosses a threshold value. $\mathrm{Re}(k)$ displays a continuous evolution while $\mathrm{Im}(k)$ is suddenly switched on for energies below the threshold. The evanescent modes allow the investigation of spin and density distributions around inhomogeneities and at interfaces in quantum wires with extended spin-orbit coupling, a condition met in many spintronic devices.

We also reviewed recent work on the influence of a localized Rashba scattering center (Rashba dot) on the linear conductance of a quantum wire. The Rashba dot sustains quasi-bound states that interfere with direct transmission along the wire and lead to Fano-resonance profiles in the energy dependence of the linear conductance. This Fano-Rashba effect was elucidated with numerical calculations using a grid discretization of the 2D Schrödinger equation and a coupled-channel model that allows a more transparent physical interpretation. This model yields analytical expressions within the ansatz approach that clearly show the appearance of the Fano function for the transmission. The validity of the ansatz solution and the truncation to the lowest two modes was assessed by finding the numerical solution of the multimode coupled-channel-model equations. Finally, we stressed that the conductance modulations obtained by varying the intensity of the local Rashba coupling seem promising as candidates for device operation in spintronics.

Acknowledgements

I gratefully thank R. López and D. Sánchez from the University of the Balearic Islands for the many fruitful discussions and scientific exchanges leading to the studies reviewed in this paper. This study was supported by the Spanish grants PCTIB-2005GC3-02 (Govern de les Illes Balears) and FIS2005-02796 (MEC) and FIS2008-00781 (MEC).

References

[1] Datta, S. Electronic Transport in Mesoscopic Systems. Cambridge (UK): Cambridge University Press, 1995 (Cambridge Studies in Semiconductor Physics and Microelectronic Engineering, 3).

[2] Ferry, D.K., Goodnick, S.M. Transport in Nanostructures. Cambridge (UK): Cambridge University Press, 1997. (Cambridge Studies in Semiconductor Physics and Microelectronic Engineering, 6).

[3] Landauer, R. IBM Journal of Research Developments **1**, 223 (1957).

[4] van Wees, B.J., van Houten, H., Beenakker, C., Willimason, J.G. Kouwenhoven, L.P., van der Marel, D., Foxon, C.T. Physical Review Letters **60**, 848 (1988)

[5] Wharam, D.A., Thornton, T.J., Newbury, R., Pepper, M., Ritchie, H., Jones, G.A.C. Journal of Physics C **21**, L209 (1988).

[6] Gurvitz, S.A., Levinson, Y.B. Physical Review B **47**, 10578 (1993).

[7] Nöckel, J.U., Stone, A.D., Physical Review B **50**, 17415 (1994).

[8] Thomas, K.J., Nicholls, J.T., Simmons, M.Y., Pepper, M., Mace, D.R., Ritchie, D.A. Physical Review Letters **77**, 135 (1996).

[9] Serra, L., Sánchez, D., López, R. Physical Review B **72**, 235309 (2005).

[10] Sánchez, D., Serra, L. Physical Review B **74**, 153313 (2006).

[11] Serra, L., Sánchez, D. Journal of Physics: Conference Series **61**, 1037 (2007).

[12] Serra, L., Sánchez, D., López, R. Physical Review B **76**, 045339 (2007).

[13] Bychkov, Y., Rashba, E.I. Journal of Physics C **17**, 6039 (1984).

[14] Winkler, R. *Spin-orbit coupling effects in two-dimensional electron and hole systems*. Berlin (Ger), Springer Verlag, 2003.

[15] Nitta, J., Akazaki, T., Takayanagi, H., Enoki, T. Physical Review Letters **78**, 1335 (1997).
[16] Datta, D., Das, B. Applied Physics Letters **56**, 665 (1990).
[17] Streda, P., Seba, P. Physical Review Letters **90**, 256601 (1990).
[18] Egues, J.C., Burkard, G., Loss, D. Physical Review Letters **89**, 176401 (2003).
[19] Nesteroff, J.A., Pershin, Yu.V., Privman, V., Physical Review Letters **93**, 126601 (2004).
[20] Bagwell, P., Physical Review B **41**, 10354 (1990).
[21] Khodas, M., Shekter, A., Finkel'stein, A.M. Physical Review Letters **92**, 086602 (2004).
[22] Valín-Rodríguez, M., Puente, A., Serra, L. Nanotechnology **14**, 882 (2003).
[23] Zhang, L., Brusheim, P., Xu, H.Q. Physical Review B **72**, 045347 (2005).
[24] Pályi, A., Péterfalvi, C., Cserti, J. Physical Review B **74**, 073305 (2006)
[25] Governale, M., Zülicke, U. Physical Review B **66**, 073311 (2002).
[26] Sinova, J., Culcer, D., Niu, Q., Sinitsyn, N.A., Jungwirth, T., MacDonald, A.H. Physical Review Letters **92**, 126603 (2004).
[27] Usaj, G., Balseiro, C.A. Europhysics Letters **72**, 635 (2005).
[28] Fano, U. Physical Review **124**, 1866 (1961).
[29] Adair, R.K., Bokelman, C.K., Peterson, R.E. Physical Review **76**, 308 (1949).
[30] Cerdeira, F., Fjeldly, T.A., Cardona, M. Phys. Rev. B **8**, 4734 (1973).
[31] Göres,J., *et al.* Physical Review B **62**, 2188 (2000).
[32] Lent, C.S., Kirkner, D.J. Journal of Applied Physics **67**, 6353 (1990).
[33] Molenkamp, L.W., Schmidt, G., Bauer, G.E.W. Physical Review B **64**, 121202(R) (2001).
[34] Sánchez, D., Serra, L., Choi, M.S. Physical Review B **77**, 035315 (2008).
[35] López, R., Sánchez, D., Serra, L. Physical Review B **76**, 035307 (2007).

About the author

Llorenç Serra *is professor of the Department of Physics at the Universitat de les Illes Balears (UIB) since 1996 and researcher in the Institute for Cross-Disciplinary Physics and Complex Systems (IFISC), created in 2007 at this same university. His research interests are the structural and dynamical properties of small-dimension systems for which quantum effects are relevant, particularly, atomic aggregates, quantum dots and semiconductor nanostructures.*